Results in Physics 8 (2018) 404–414

Contents lists available at ScienceDirect

Results in Physics

journal homepage: www.journals.elsevier.com/results-in-physics

Heat generation/absorption and nonlinear radiation effects on stagnation point flow of nanofluid along a moving surface

Feroz Ahmed Soomro [a], Rizwan Ul Haq [b], Qasem M. Al-Mdallal [c,*], Qiang Zhang [a]

[a] Department of Mathematics, Nanjing University, Nanjing 210093, China
[b] Department of Electrical Engineering, Bahria University, Islamabad, Pakistan
[c] Department of Mathematical Sciences, United Arab Emirates University, Al-Ain, United Arab Emirates

ARTICLE INFO

Article history:
Received 23 October 2017
Received in revised form 10 December 2017
Accepted 14 December 2017
Available online 20 December 2017

Keywords:
Heat generation/absorption
Nonlinear thermal radiation
Nanofluid
Stagnation point
Convective boundary
Numerical solution

ABSTRACT

In this study, heat generation/absorption effects are studied in the presence of nonlinear thermal radiation along a moving slip surface. Uniform magnetic field and convective condition along the stretching surface are adjusted to deal the slip mechanisms in term of Brownian motion and thermophoresis for nanofluid. The mathematical model is constructed in the form of coupled partial differential equations. By introducing the suitable similarity transformation, system of coupled nonlinear ordinary differential equations are obtained. Finite difference approach is implemented to obtain the unknown functions of velocity, temperature, nanoparticle concentration. To deduct the effects at the surface, physical quantities of interest are computed under the effects of controlled physical parameters. Present numerical solutions are validated via numerical comparison with existing published work for limiting cases. Present study indicates that due to increase in both Brownian motion and thermophoresis, the Nusselt number decreases while Sherwood number shows the gradual increase.

Introduction

After the initial concept of boundary layer theory, Sakiadis presented the series of articles [1–3] in 1961, where he mentioned the new class of boundary layer problems that deals the flow on a continuous solid surface. In his study, mathematical model and their solutions were proposed for continuous flat and cylindrical surfaces. The work was further extended by Crane [4] in which he deals the flow past a stretching surface. Study of such kind of flows got motivation from its application point of view, particularly in drawing of plastic films. Therefore, many researchers paid much attention to this problem and investigated boundary layer flow over different kinds of stretching surfaces. Literature depicts that two-dimensional stagnation-point flow towards a stretching surface was first studied by Chiam [5]. He considered the same velocity at the stretching surface and away from surface. But there may be physical situation where the ambient velocity of fluid flow and at the stretching surface is different. So, Mahapatra and Gupta [6] revisited the same problem and considered different ambient and stretching velocity. Since the researchers have taken keen interest into the study of stagnation-point flow over different kinds of stretching surfaces. Few relevant studies are: unsteady MHD mixed convection slip flow over nonlinearly stretching sheet presented by Shen et al. [7]. Flow of axisymmetric stagnation-point flow over vertical stretching sheet is studied by Khuzaimah et al. [8] and similarly stagnation-point flow of nanofluid over inclined stretching sheet was discussed by Animasaun et al. [9]. In non-Newtonian class, unsteady micropolar fluid over curved stretching sheet presented by Choi and Eastman [10].

Despite of being many industrial applications of nanofluid and nanoparticles there are several universal applications including: nuclear systems cooling, heat transfer intensification, electronic applications, transportation, industrial cooling applications, heating buildings and reducing pollution, space and defense, mass transfer enhancement, solar absorption, energy storage, friction reduction, magnetic sealing, magnetic fluids (ferromagnetic fluid), biomedical application, antibacterial activity, nanofluids as vehicular brake fluids, nanofluids-based microbial fuel cell, etc. Different from conventional fluids the nanofluids has acquired considerable position in the field of science and industry. The use of nanofluid has been used to control the various thermo physical properties of fluids used in engineering and science industry, for example, heat transfer capacity, thermal heat rate, thermal conductivity, etc., which are very important to improve the performance of the working objects. In comparison to conventional base fluids, the nanoparticle contained fluids has shown enhancement of heat transfer and thermal conductivity [11,12]. For detailed survey that

* Corresponding author.
E-mail address: q.almdallal@uaeu.ac.ae (Q.M. Al-Mdallal).

https://doi.org/10.1016/j.rinp.2017.12.037
2211-3797/

deals the applications of nanofluids are referred to Kuafui and Omar [13]. Nanoparticles of nanometer sized (about 1–100 nm) are combined with the conventional base fluids, like water, engine oil, glycol, etc., to make such mystical nanofluid which has revolutionized the industry recently. Apart from other field, nanofluid in the field of heat transfer has also been studied and analyzed under various situations. Initial study of nanofluid flow along a stretching sheet is presented by Khan and Pop [14]. After that, stagnation-point flow of nanofluid over stretching sheet with slip and radiation effects are modified by Haq et al. [15]. Metallic nanoparticles (Cu and Al_2O_3) based nanofluid flow over stretching sheet with inclined magnetic field effects recently studied by Rashid et al. [16]. Water driven copper nanoparticles nanofluid axisymmetric flow and stream wise flow are studied by Haq et al. [17,18].

In the usual circumstances velocity of the fluid at the boundary is considered as negligible so it is taken as zero but to better understand the dynamics of fluids at nano scale it is crucial to consider such velocity called slip velocity. In this context many different kinds of velocity slip models have been proposed. Few popular and recently interested studies includes by Fukui and Kaneko [19] for Poiseuille flow rates with high knudsen number lubrication Problem. Similarly, 1.5-order velocity slip is discussed by Mitsuya [20]. Rarified gases arising from inequalities of temperature is obtained by Maxwell [21] and second-order velocity slip model for rarefied gas flows is discussed by Wu [22]. Mass transfer induced velocity slip model is carried out by Wu [23]. Reported results in the literature depicts that velocity slip has considerable impact on the flow and heat transfer characteristics. Few recently reported related studies are [24,25].

Recently many researchers have studied the thermal radiation on the flow and heat transfer characteristics of both conventional and nanofluids over stretching surfaces. For example, effects of nonlinear thermal radiation on the Williamson nanofluid flow over stretching surface were studied by Kumar et al. [26]. Buoyancy flow of nanofluid over the vertical stretching sheet under the effects of thermal radiation was investigated by Dogonchi and Ganji [27]. Both of these studies considered steady state flow of fluid. Besides, thermal radiation effects on the unsteady stagnation-point flow of magneto-hydrodynamic fluid towards the shrinking sheet were studied by [28]. Effects of thermal radiation on the flow and heat transfer over the nonlinear stretching sheet were reported by [29]. Effects of thermal radiation on flow and heat transfer over moving surface were discussed by Mohamed and Wahed [30]. Nonlinear thermal radiation effects on the oblique stagnation point flow over towards horizontal stretching sheet were reported in [31–33].

Motivated from the work cited above, the focus of present study is to investigate the effects of velocity slip and nonlinear radiation on the flow and heat transfer of magnetohydrodynamic stagnation-point nanofluid flow over convective stretching sheet. To the best of our knowledge, such study has not been reported yet. For validation of present results, comparison is made with the previously reported results in the limiting case. All the results are thoroughly analyzed and presented through tables and graphs.

Problem formulation

Let us consider two-dimensional stagnation-point flow of a nanofluid over convective stretching surface which is stretched in both directions with the linear constant velocity $u = u_w(x) = ax$, where a is an arbitrary constant, along the horizontal $x-axis$. Moreover, the velocity of the fluid in the ambient boundary layer region is considered as $u = u_\infty(x) = cx$, where c is arbitrary constant. The nanofluid flow along the $y-axis$ and meets the horizontal stretching sheet at the origin. As a result the fluid is divided into two streams leaving in positive and negative x directions, respectively. Uniform magnetic field of strength B_0 is applied normal to the stretching surface. Under the above mentioned conditions and after applying necessary boundary layer approximations, the governing boundary layer equations may be written as

$$\frac{\partial u}{\partial x}+\frac{\partial u}{\partial y}=0 \tag{1}$$

$$u\frac{\partial u}{\partial x}+v\frac{\partial u}{\partial y}=u_\infty\frac{\partial u_\infty}{\partial x}+\vartheta\frac{\partial^2 u}{\partial y^2}+\frac{\sigma B_0^2}{\rho}(u_\infty-u) \tag{2}$$

$$u\frac{\partial T}{\partial x}+v\frac{\partial T}{\partial y}=\frac{\partial}{\partial y}\left(\alpha\frac{\partial T}{\partial y}-\frac{1}{\rho C_p}q_r\right)+\frac{\vartheta}{C_p}\left(\frac{\partial u}{\partial y}\right)^2+\tau D_B\frac{\partial C}{\partial y}\frac{\partial T}{\partial y}+\frac{\tau D_T}{T_\infty}\left(\frac{\partial T}{\partial y}\right)^2+\frac{\sigma B_0^2}{\rho C_p}(u-u_\infty)^2+Q(T-T_\infty) \tag{3}$$

$$u\frac{\partial C}{\partial x}+v\frac{\partial C}{\partial y}=D_B\left(\frac{\partial^2 C}{\partial y^2}\right)+\frac{D_T}{T_\infty}\left(\frac{\partial^2 T}{\partial y^2}\right) \tag{4}$$

with the boundary conditions

$$y=0\Rightarrow\begin{cases}u=u_w+U_{slip}\\ v=0\\ -k_f\frac{\partial T}{\partial y}=h_f(T_f-T)\\ C=C_w\end{cases},\quad y\to\infty\Rightarrow\begin{cases}u\to u_\infty\\ T\to T_\infty\\ C\to C_\infty\end{cases} \tag{5}$$

where, u and v are the velocity components along x and $y-axis$, respectively, ϑ is the kinematic viscosity of nanofluid, σ is the electrical conductivity of the nanofluid, ρ density of the nanofluid, T and T_∞ are the temperature of nanofluid and temperature of nanofluid in ambient region, respectively, α is the thermal diffusivity of nanofluid, C_p is the specific heat capacity of nanofluid, $\tau=(\rho C)_p/(\rho C)_f$ is the ratio between the effective heat capacity of the nanoparticle materials and heat capacity of the base fluid, D_B is the Brownian diffusion coefficient, D_τ is the thermophoresis diffusion coefficient, Q is the rate of heat generation/absorption, C and C_∞ are the nanoparticle concentration and nanoparticle concentration in the ambient region, respectively. U_w is the slip condition at the stretching sheet and the radiative heat flux q_r is given as

$$q_r=-\frac{4\sigma^*}{3k^*}\frac{\partial T^4}{\partial y}=-\frac{16\sigma^*}{3k^*}T^3\frac{\partial T}{\partial y}. \tag{6}$$

In the above expression, σ^* and k^* are stefan-Boltzman constant and mean absorption coefficient, respectively. Now introducing the temperature $\theta(\eta)=(T-T_\infty)/(T_f-T_\infty)$ in term of $T=T_\infty(1+(\theta_w-1)\theta)$. Where, $\theta_w=T_f/T_\infty$ (temperature parameter). First term of right hand side of Eq. (3) can also be expressed as $\alpha\frac{\partial}{\partial y}\left\{\frac{\partial T}{\partial y}(1+R_d(1+(\theta_w-1)\theta)^3)\right\}$, where $R_d=-\frac{16\sigma^*T_\infty^3}{3kk^*}$.

Using the following similarity transformation variable

$$f(\eta)=\frac{\psi}{x\sqrt{a\vartheta}},\theta(\eta)=\frac{T-T_\infty}{T_f-T_\infty},\phi(\eta)=\frac{C-C_\infty}{C_w-C_\infty},\eta=\sqrt{\frac{a}{\vartheta}}y \tag{7}$$

where ψ is the similarity function which is defined as $u=\partial\psi/\partial y$ and $v=-\partial\psi/\partial x$, the Eqs. (1–5) are converted into the following system of ordinary nonlinear differential equations

$$f'''(\eta)+f(\eta)f''(\eta)-(f'(\eta))^2+M(\varepsilon-f'(\eta))+\varepsilon^2=0 \tag{8}$$

$$\frac{1}{\Pr}\frac{d}{d\eta}[(1+R_d(1+(\theta_w-1)\theta(\eta))^3)\theta'(\eta)]+f(\eta)\theta'(\eta)+Ec(f''(\eta))^2+M(\varepsilon-f'(\eta))^2Ec+\lambda\theta(\eta)+N_b\phi'(\eta)\theta'(\eta)+N_t(\theta'(\eta))^2=0\Big\} \tag{9}$$

$$\phi'' + Le\Pr f\phi' + \frac{N_t}{N_b}\theta'' = 0 \tag{10}$$

subject to the boundary conditions

$$\eta = 0 \Rightarrow \begin{cases} f'(0) = 1 + Kf''(0) \\ f(0) = 0 \\ \theta'(0) = -\gamma[1-\theta(0)] \\ \phi(0) = 1 \end{cases}, \quad \eta \to \infty \Rightarrow \begin{cases} f'(\infty) \to \varepsilon \\ \theta(0) = 0 \\ \phi(0) = 0 \end{cases} \tag{11}$$

where Magnetic number M, velocity ratio parameter ε, Prandtl number Pr, Radiation parameter R_d, temperature ratio parameter θ_w, Eckert number Ec, source/sink parameter λ, Brownian motion parameter N_b, thermophoresis parameter N_t, Lewis number Le, velocity slip parameter K and Biot number γ are defined as

$$K = l\sqrt{\frac{a}{\vartheta}}, M = \frac{\sigma B_0^2}{\rho a}, \Pr = \frac{\vartheta}{\alpha}, Le = \frac{\vartheta}{D_B}, \gamma = \frac{h_f}{k}\sqrt{\frac{\vartheta}{a}}, \ Ec = \frac{u_w^2}{C_p(T-T_\infty)},$$
$$\varepsilon = \frac{b}{a}, \lambda = \frac{Q}{(\rho C_p)\alpha}, \theta_w = \frac{T_f}{T_\infty}, N_b = \frac{(\rho C_p)D_B(C-C_\infty)}{(\rho C_p)\vartheta},$$
$$N_t = \frac{(\rho C_p)D_R(T-T_\infty)}{(\rho C_p)\vartheta T_\infty} \tag{12}$$

Apart from temperature distribution and fluid velocity, the other quantities of physical interest are the friction at the stretching surface, heat transfer rate and mass transfer rate which are given by coefficient of skin friction C_f, Nusselt number Nu and Sherwood number Sh and are defined as

$$C_f = \frac{\tau_w}{\rho u_w^2}, Nu = \frac{xq_w}{k(T_w - T_\infty)}, Sh = \frac{xq_m}{D_B(C_w - C_\infty)} \tag{13}$$

where,

$$\tau_w = \mu\left(\frac{\partial u}{\partial y}\right)_{y=0}, q_w = -k\left(\frac{\partial T}{\partial y}\right)_{y=0} + (q_r)_w, q_m = D_B\left(\frac{\partial C}{\partial y}\right)_{y=0} \tag{14}$$

Using (14) into (13) and after simplification we get the following non dimensional form for reduced coefficient of skin friction, Nusselt number and Sherwood number

$$\frac{1}{2}C_f\sqrt{2\mathrm{Re}_x} = f''(0), \quad \mathrm{Re}_x^{-1/2}Nu = -[1 + R_d\theta_w^3]\theta'(0),$$
$$\mathrm{Re}_x^{-1/2}Sh = -\phi'(0) \tag{15}$$

Methodology

The system of coupled nonlinear ordinary differential Eqs. (8) (10) along with the boundary conditions (11) were solved using finite difference method (FDM). The uniform step size of 10^{-5} and truncation error tolerance of 10^{-8} was used in the computation. After initial experimental analysis it was concluded to restrict the infinite domain to show the convergence of the solutions profiles. The detailed analysis is presented in the following paragraphs. In order to show the validity of present solutions, the comparison is made with the already reported results in the limiting case. Table 1 and 2 shows the achievement of good comparison with the results reported results by Khan and Pop [14].

Results and discussion

In order to determine the results of unknown functions of velocity, temperature and concentration we have plotted the results in Figs. 1–17. Fig. 1 depicts the profiles of velocity of nanofluid against under the effects of magnetic parameter M, velocity ratio parameter ε and slip parameter K. It is evident from the trends of the profiles that increasing value of magnetic parameter M produces decrease in the velocity $f'(\eta)$ of nanofluid whereas inverse trends of profiles can be seen for the increasing value of velocity ratio parameter ε. Moreover, velocity slip parameter K has different effects on the velocity of nanofluid in the different range value of velocity ratio parameter ε. Fig. 1(b) clearly shows that in the range $\varepsilon > 1$, increasing value of slip parameter produces increase in the velocity of nanofluid whereas reverse behavior can be witnessed for the value of velocity ratio parameter in the range $\varepsilon < 1$. It should be noted that there is not effect of the velocity of nanofluid due to change in the value of slip when $\varepsilon = 1$. It is also evident from the Fig. 1 that momentum boundary layer thickness tends to increase as the magnetic effects are increased. Due to increasing value of slip parameter the momentum boundary layer thickness is decreased for the range $\varepsilon > 1$ of velocity ratio parameter and inverse trend of profiles is observed in the range $\varepsilon < 1$.

Fig. 2, presents the profiles of temperature distribution $\theta(\eta)$ under the effects of thermal radiation R_d, Brownian motion N_b and thermophoresis N_t. It can be seen from the profile trends that temperature of nanofluid $\theta(\eta)$ always tends to increase for increasing value of Brownian motion parameter N_b and thermophoresis parameter N_t under the effects of thermal radiation R_d. As the effects of thermal radiation R_d are increased thermal boundary layer thickness tends to decrease. Moreover, in the absence of thermal radiation R_d, it can be seen that thermal boundary layer thickness is decreased due to increasing value of Brownian motion parameter N_b and inverse trend is observed for the increasing value of thermophoresis parameter N_t.

Table 1
Comparison with previously published data for the values of $\mathrm{Re}_x^{-1/2}\,Nu_x$, when $M = Rd = Ec = \varepsilon = \lambda = K = 0$ and $\gamma \to \infty$, when $\Pr = 10$ and $Le = 1$.

	$N_b = 0.1$ Khan [14]	$N_b = 0.1$ Present study	$N_b = 0.3$ Khan [14]	$N_b = 0.3$ Present study	$N_b = 0.5$ Ref [14]	$N_b = 0.5$ Present study
$N_t \downarrow$	$-\theta'(0) \downarrow$	$-\theta'(0) \downarrow$	$-\theta'(0) \downarrow$	$-\theta'(0) \downarrow$	$-\theta'(0) \downarrow$	$-\theta'(0) \downarrow$
0.1	0.9524	0.95247	0.2522	0.25223	0.0543	0.05433
0.3	0.5201	0.52013	0.1355	0.13554	0.0291	0.02918
0.5	0.3211	0.32110	0.0833	0.08336	0.0179	0.01794

Table 2
Comparison with previously published data for the values of $\mathrm{Re}_x^{-1/2}\,Sh$, when $M = Rd = Ec = \varepsilon = \lambda = K = 0$ and $\gamma \to \infty$, when $\Pr = 10$ and $Le = 1$.

	$N_b = 0.1$ Khan [14]	$N_b = 0.1$ Present study	$N_b = 0.3$ Khan [14]	$N_b = 0.3$ Present study	$N_b = 0.5$ Khan [14]	$N_b = 0.5$ Present study
$N_t \downarrow$	$-\phi'(0) \downarrow$	$-\phi'(0) \downarrow$	$-\phi'(0) \downarrow$	$-\phi'(0) \downarrow$	$-\phi'(0) \downarrow$	$\phi'(0) \downarrow$
0.1	2.1294	2.12946	2.4100	2.41002	2.3836	2.38362
0.3	2.5286	2.52861	2.6088	2.60881	2.4984	2.49847
0.5	3.0351	3.03515	2.7519	2.75199	2.5731	2.57313

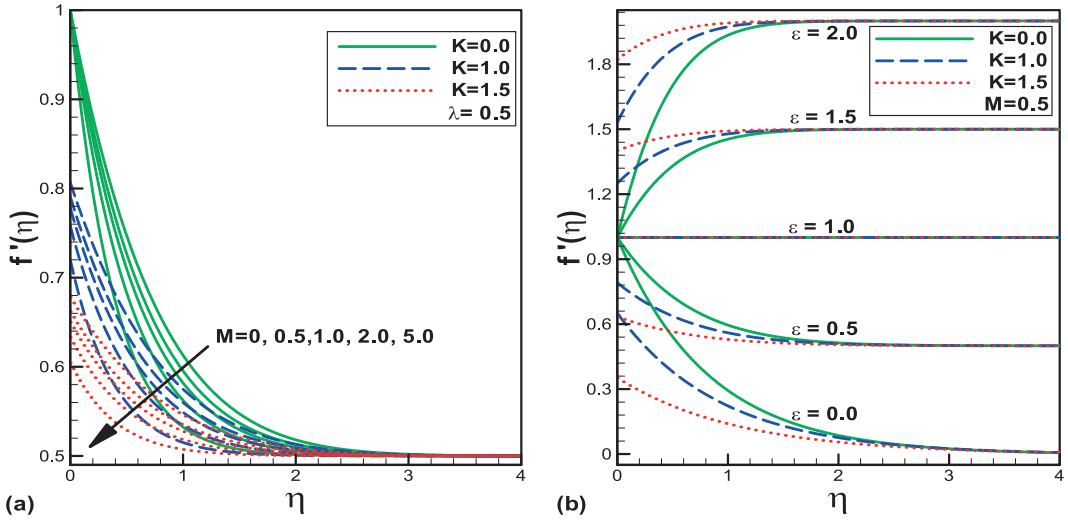

Fig. 1. Variation of velocity for various values of (a) M and K (b) ε and K.

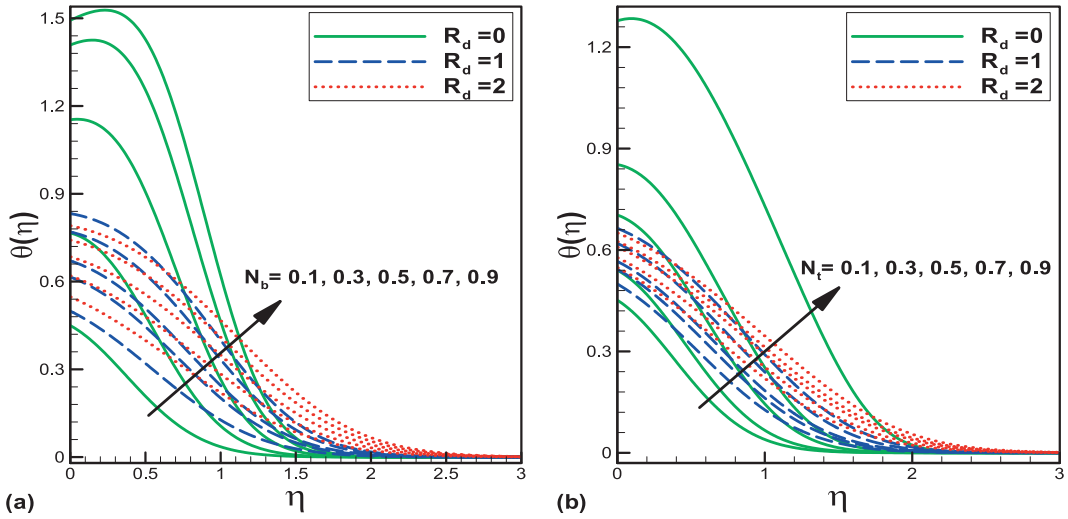

Fig. 2. Variation of temperature for various values of (a) N_b and R_d (b) N_t and R_d.

Fig. 3 shows the profiles of nanoparticle concentration $\phi(\eta)$ under the effects of thermal radiation R_d, Brownian motion N_b and thermophoresis N_t. The profiles $\phi(\eta)$ depicts that concentration of nanoparticle is decreased due to increasing value of Brownian motion parameter N_b and thermal radiation parameter R_d and increased due to increasing value of thermophoresis parameter N_t. In the absence of thermal radiation R_d, nanoparticle concentration boundary layer thickness is decreased due to increasing value of Brownian motion parameter N_b whereas inverse trend is observed due to increasing value of thermophoresis parameter N_t.

Fig. 4(a) and (b) shows the profiles of temperature distribution $\theta(\eta)$ and nanoparticle concentration $\phi(\eta)$ under the magnetic M and thermal radiation effect R_d. It is evident that both temperature $\theta(\eta)$ and nanoparticle concentration $\phi(\eta)$ is increased due to increasing value of magnetic parameter M. That is due to the fact that velocity of the nanofluid $f'(\eta)$ is decreasing due to higher value of magnetic parameter M so results of temperature and concentration of nanoparticles increase within the temperature $\theta(\eta)$ and nanoparticle concentration $\phi(\eta)$.. In the absence of thermal radiation R_d, the thermal and concentrate domain ion boundary layer thickness tends to increase due to increasing effects of magnetic parameter M. Fig. 5(a) and (b) shows the effects of slip parameter K on the temperature $\theta(\eta)$ and nanoparticle volume fraction $\phi(\eta)$. It can be seen that the temperature $\theta(\eta)$ and nanoparticle volume fraction $\phi(\eta)$ is increased due to increase in slip K whereas thermal and nanoparticle boundary layer thickness is decreased. It is due to the fact that velocity $f'(\eta)$ of the nanofluid is decreased due to increase in slip parameter K thus less heat and nanoparticles are transported which give produces increase in temperature $\theta(\eta)$ and nanoparticle volume fraction $\phi(\eta)$. It is also seen that increasing value of radiation parameter R_d gives rise to temperature $\theta(\eta)$ whereas inverse effect are reported on nanoparticle volume fraction $\phi(\eta)$.

Effects of source/sink parameter on the temperature and nanoparticle volume fraction are given by Fig. 6(a) and (b). It is observed that increasing the effects of source/sink parameter produces increase in the temperature and nanoparticle volume fraction. Velocity of nanofluid and coefficient of skin friction against the increasing value of magnetic and velocity ratio parameter is given by Fig. 7(a) and (b) respectively. It shows that velocity of nanofluid at the surface of the stretching sheet tends to decrease due to increase in magnetic parameter and increased due to increase in velocity ratio parameter. On the other hand the coefficient of skin friction tends to increase due to increase in magnetic

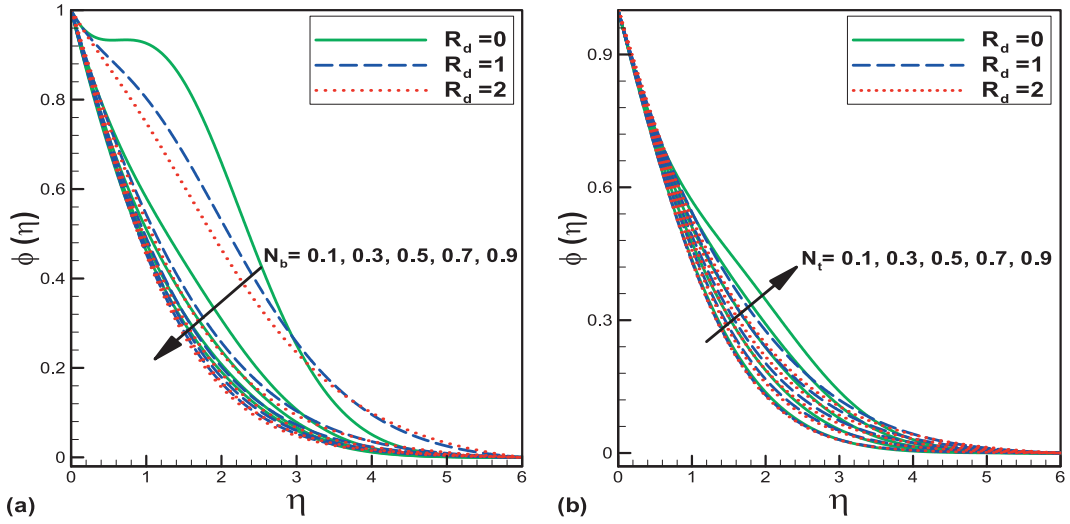

Fig. 3. Variation of nanoparticle volumetric concentration for various values of (a) N_b and R_d (b) N_t and R_d.

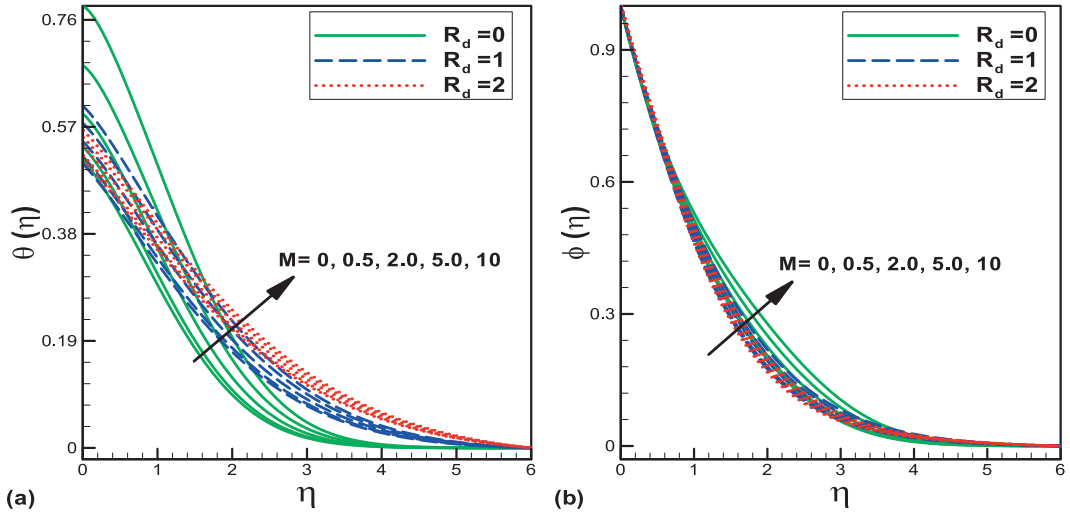

Fig. 4. Variation of (a) temperature and (b) nanoparticle volumetric concentration for various values of M and R_d.

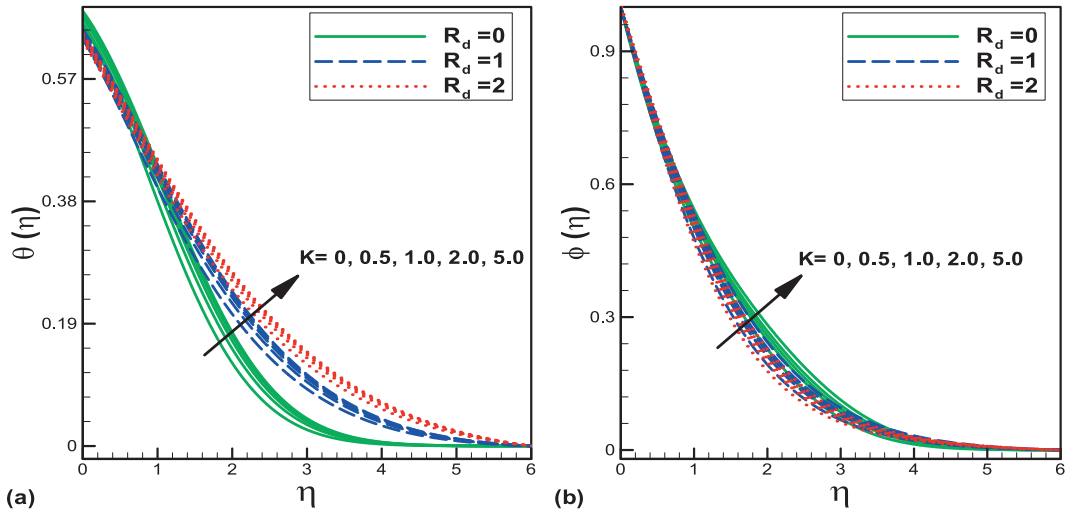

Fig. 5. Variation of (a) temperature and (b) nanoparticle volumetric concentration for various values of K and R_d.

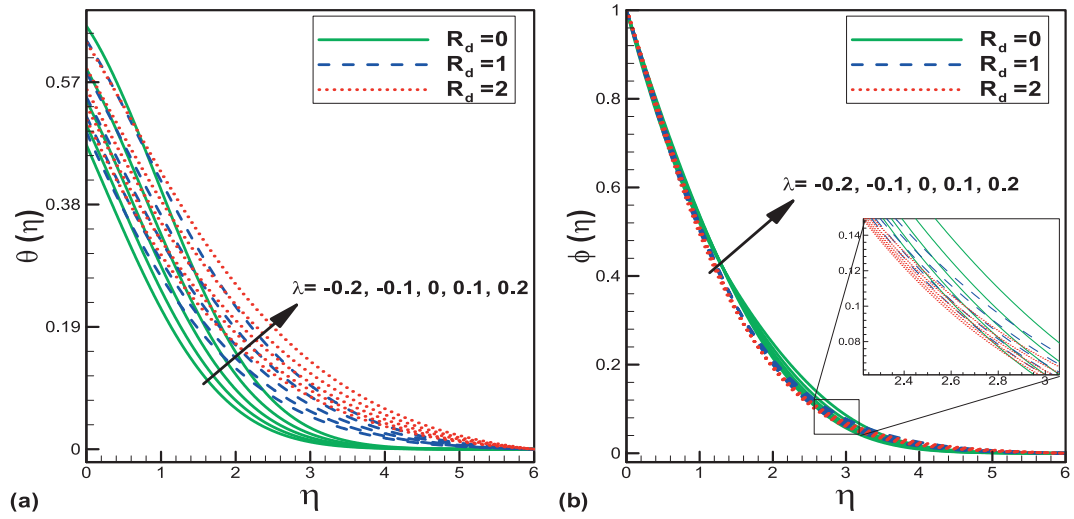

Fig. 6. Variation of (a) temperature and (b) nanoparticle volumetric concentration for various values of λ and R_d.

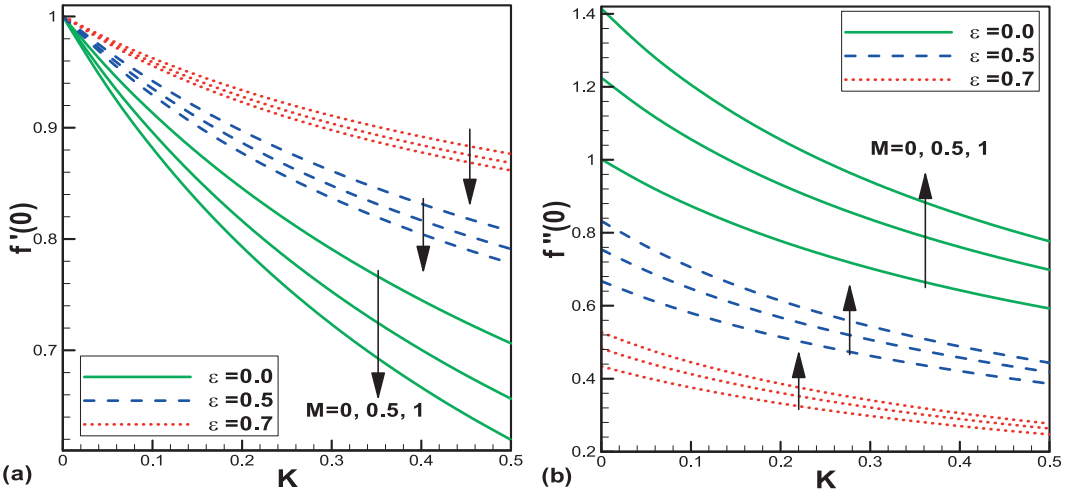

Fig. 7. Variation of (a) $f'(0)$ and (b) $f''(0)$ for various values of ε and M.

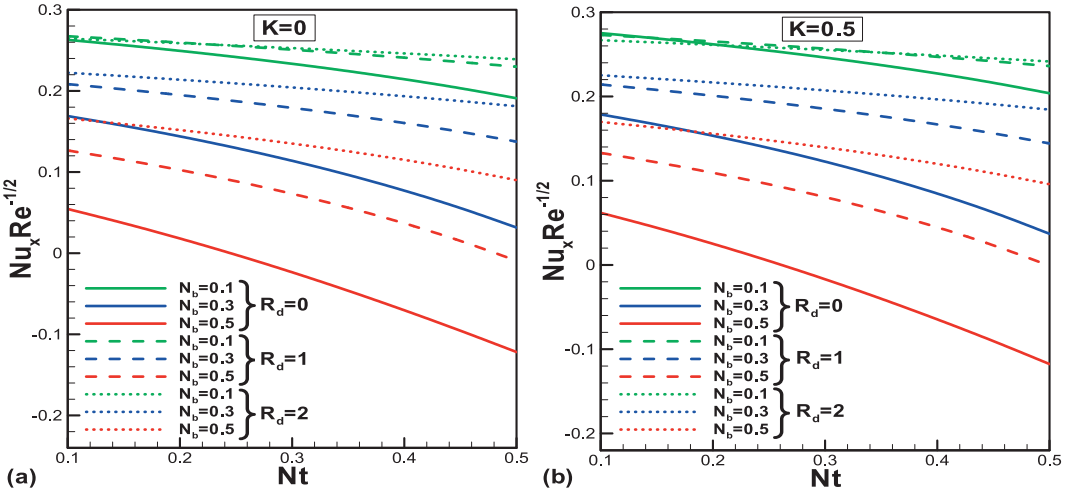

Fig. 8. Variation of Nusselt number for various values of N_b and R_d when (a) $K = 0$ and (b) $K = 0.5$.

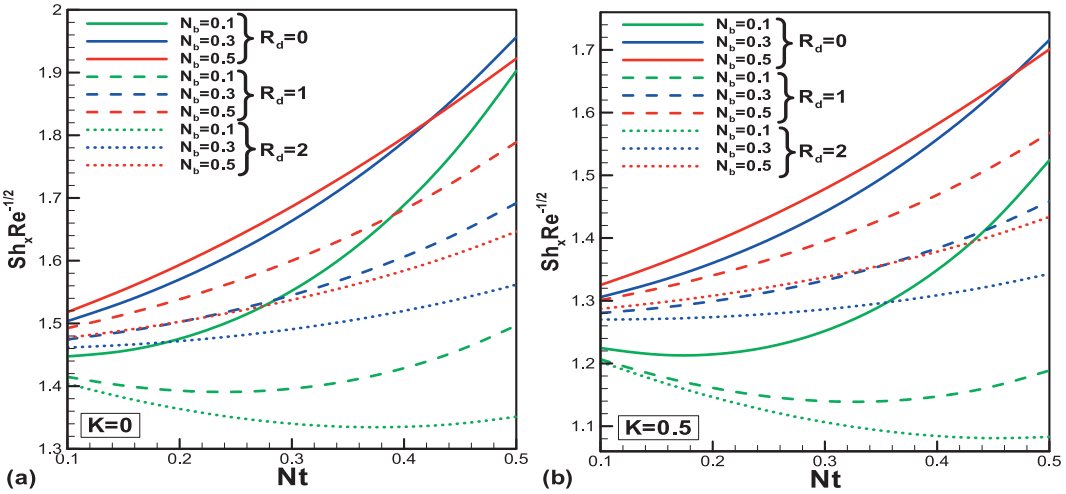

Fig. 9. Variation of Sherwood number for various values of N_b and R_d when (a) $K = 0$ and (b) $K = 0.5$.

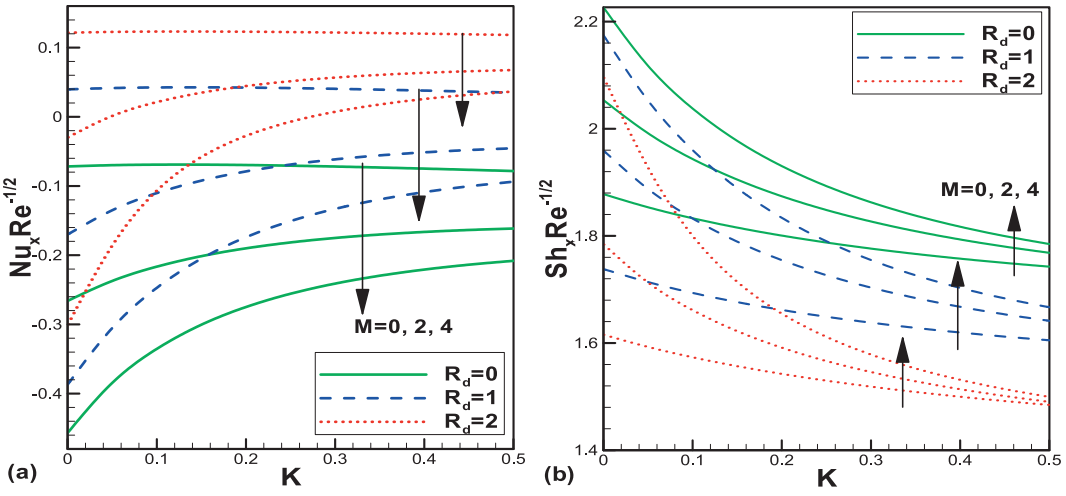

Fig. 10. Variation of (a) Nusselt number and (b) Sherwood number for various values of M and R_d.

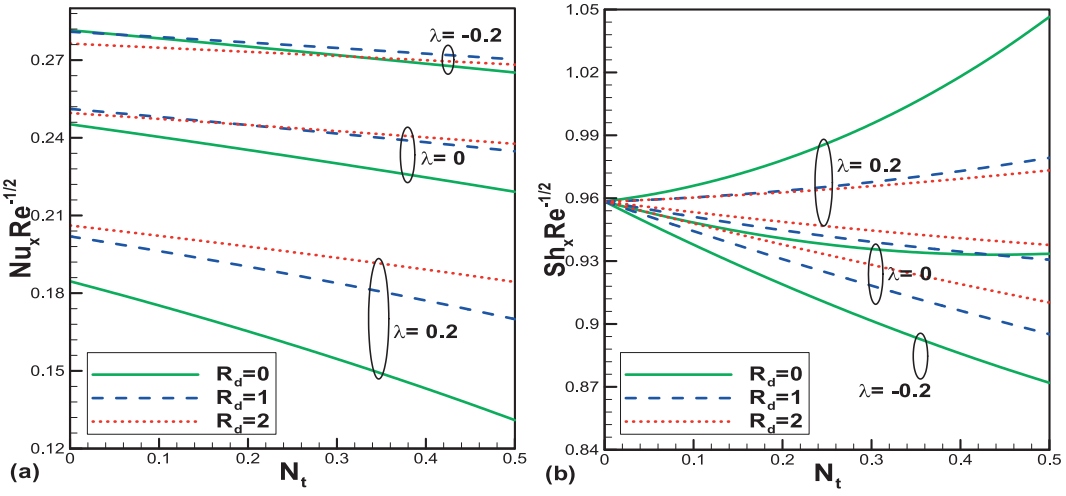

Fig. 11. Variation of (a) Nusselt number and (b) Sherwood number for various values of λ and R_d.

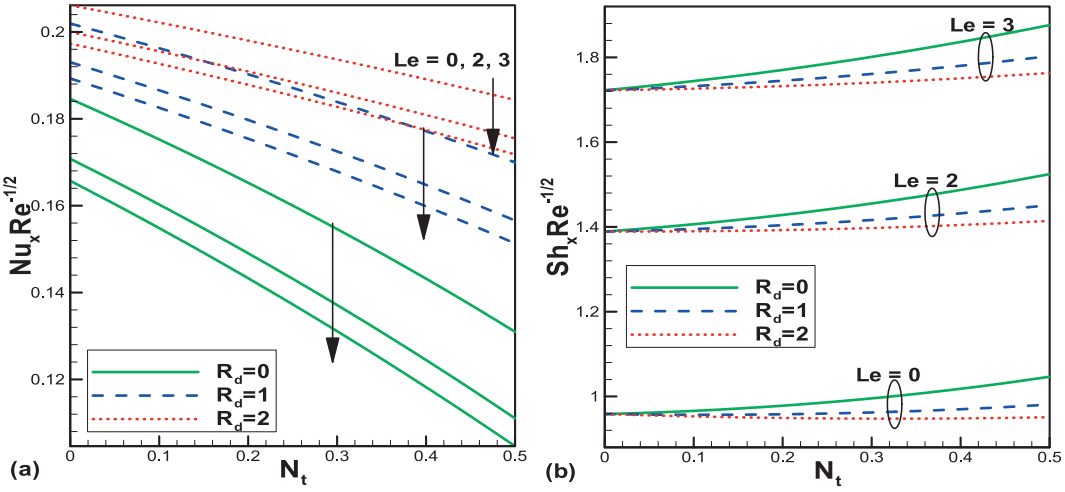

Fig. 12. Variation of (a) Nusselt number and (b) Sherwood number for various values of *Le* and R_d.

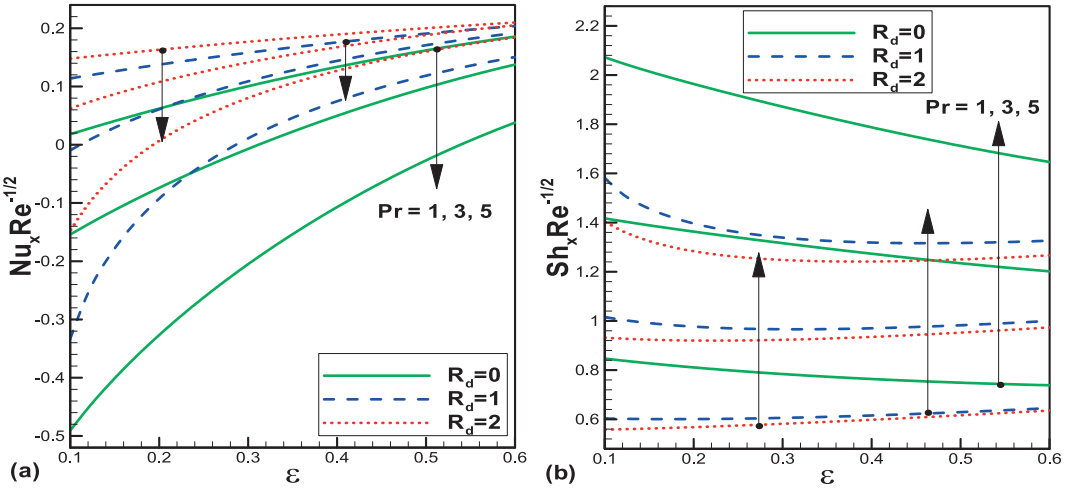

Fig. 13. Variation of (a) Nusselt number and (b) Sherwood number for various values of Pr and R_d.

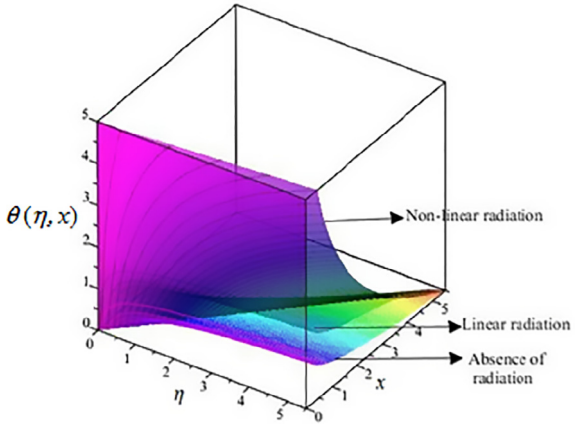

Fig. 14. Comparison of isotherms variation for linear, non-linear and absence of radiation.

parameter and decreased due to increase in velocity ratio parameter. Effect of nonlinear thermal radiation parameter, Brownian motion parameter, thermophoresis parameter and velocity slip parameter on the Nusselt number and Sherwood number is given by Figs. 8 and 9, respectively. It is clear from the trends of the profiles that Nusselt number tends to increase due to increase in nonlinear thermal radiation effects and decreases due to increase in both Brownian motion parameter and thermophoresis parameter. It is also evident that increasing the slip does not have prominent effect on the Nusselt number. On the other hand, Sherwood number is decreased due to increase in thermal radiation parameter and decreased due to increase in both Brownian motion parameter and thermophoresis parameter. Increasing the velocity slip effects reduces the Sherwood number.

The effect of magnetic parameter, thermal radiation parameter and velocity slip parameter on the Nusselt number and Sherwood number is given by Fig. 10(a) and (b) respectively. It can be seen clearly that due to increase in magnetic effects the Nusselt number tends to decrease and inverse effects can be observed in case of Sherwood number. Moreover, increasing the value of thermal radiation parameter produces increase in Nusselt number and decrease in Sherwood number. Increasing value of velocity slip parameter has increasing effect on the Nusselt number under the effect of magnetic field. In the absence of magnetic field, increasing value of slip parameter produces slight decrease in Nusselt number. On the other hand, increasing value of slip parameter always decrease in the Sherwood number but the standing out fact is that in the absence of magnetic field the decreasing effects of velocity effect

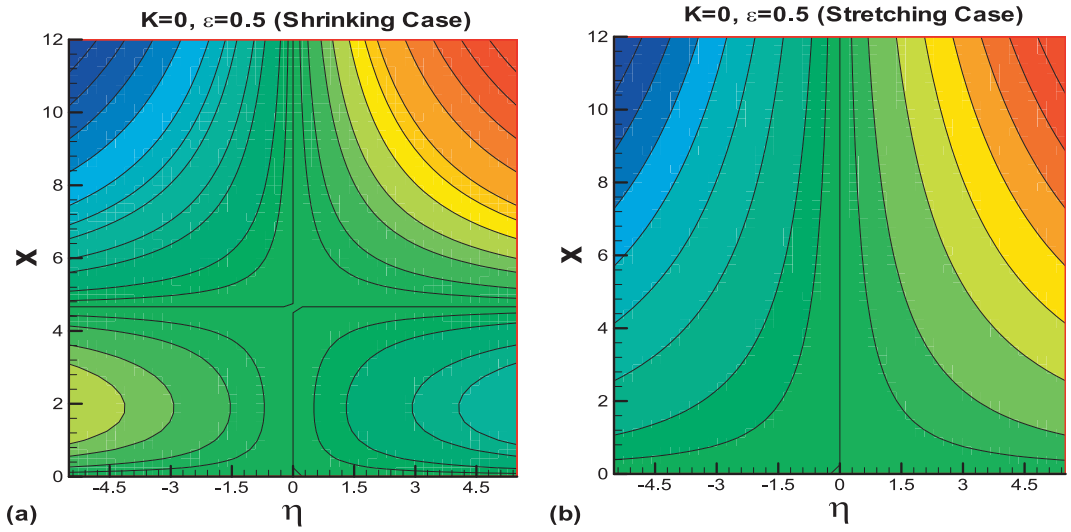

Fig. 15. Variation of stream lines for (a) shrinking case and (b) stretching case.

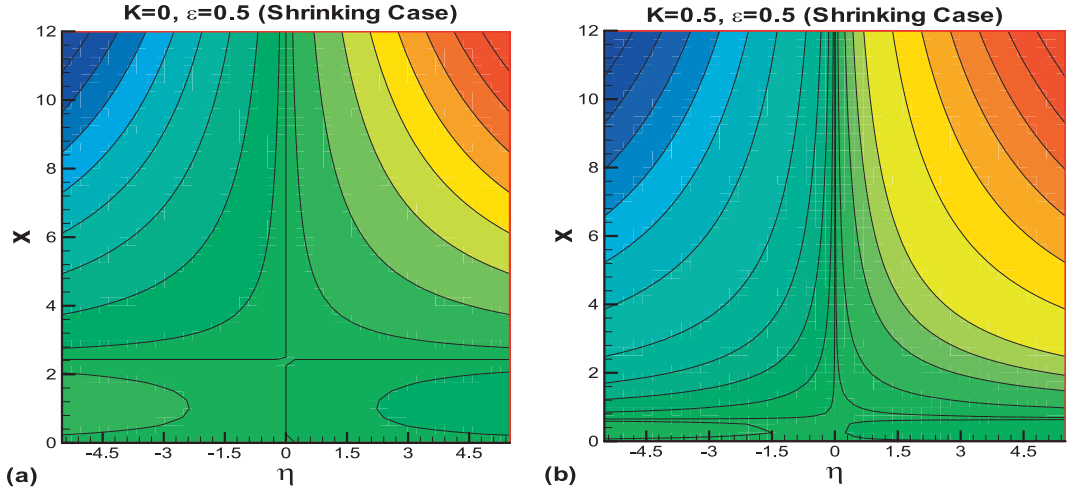

Fig. 16. Variation of stream lines for shrinking case (a) $K = 0$ and (b) $K = 0.5$.

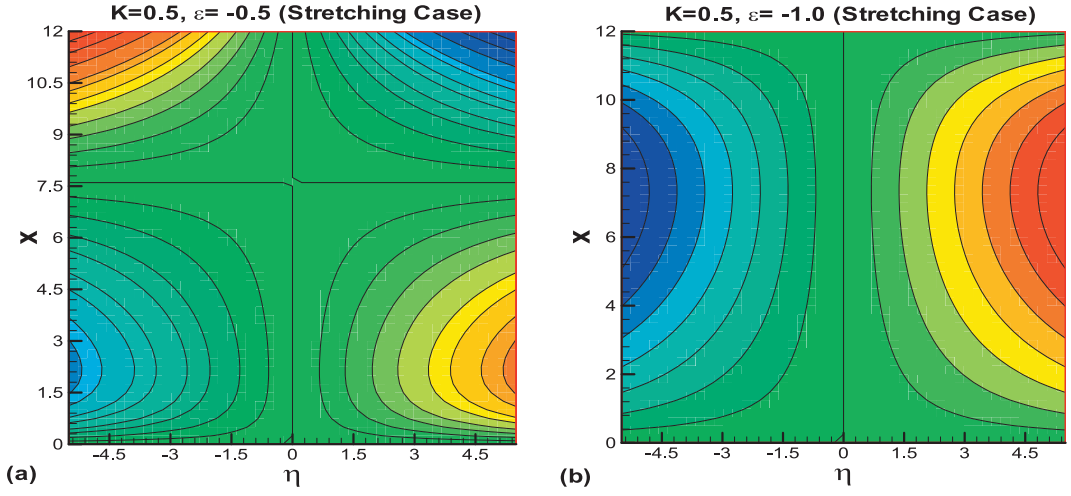

Fig. 17. Variation of stream lines for stretching case (a) $\varepsilon = -0.5$ and (b) $\varepsilon = -1.0$.

on the Sherwood number is less as compare to large value of magnetic parameter.

Effect of source/sink parameter under the effects of thermal radiation and thermophoresis parameter on the Nusselt number and Sherwood number is given by Fig. 11(a) and (b). Increase the source parameter we can notice decrease in Nusselt number and increase in Sherwood number. In the region of sink parameter, the Nusselt number is decreased due to increase in thermal radiation parameter when thermophoresis effects are neglected whereas as the thermophoresis effects are increased the Nusselt number tends to increase due to increase in thermal radiation parameter. On the other hand in the region of sink parameter, increasing value of thermal radiation parameter produces increase in Sherwood number whereas it is decreased in the region of source parameter.

Effects of Lewis number under the influence of thermal radiation and thermophoresis on the Nusselt and Sherwood number is given by Fig. 12(a) and (b), respectively. It is observed that Nusselt number is decreased due to increase in Lewis number and thermophoresis parameter whereas inverse trends can be seen due increase in the thermal radiation parameter. On the other hand Sherwood number tends to increase due to increase in Lewis number and thermophoresis whereas decreases due to increase in thermal radiation parameter. It is also observed that as the thermal radiation effects are increased the increasing value of thermophoresis parameter does not have prominent effects on the Sherwood number.

The effect of Prandtl number, velocity ratio parameter and thermal radiation on the Nusselt number and Sherwood number is given by Fig. 13(a) and (b). It can be noticed that Nusselt number is decreased due to increase in Prandtl number whereas Sherwood number is increased. Moreover, both thermal radiation and velocity ratio parameter has increasing effect on the Nusselt number. On the other hand, in the absence of thermal radiation the Sherwood number is decreased due to increase in velocity ratio parameter, whereas as the thermal radiation effects are increased the Sherwood number tends to increase due to increase in the velocity ratio parameter. Variation of isotherms describes the heat transfer in the entire domain of the given physical system (see Fig. 14). Significant effects of linear, non-linear and absence of radiation effects can be found in the three dimension behavior of isotherms and it is found that in case of non-linear radiation, heat transfer is quite dominant. In order to describe the flow behavior, stream lines are drawn for various values of emerging parameter for the entire domain of the model (see Figs. 15–17). In Fig. 15(a) and (b), results are plotted for both shrinking and stretching case of the surface for Newtonian case ($K = 0$). It can easily observed that for shrinking case flow rotation behavior near the surface is quite dominant as compare to the stretching case. Similarly in Fig. 16, we have made comparison for Newtonian ($K = 0$) and non-Newtonian case ($K = 0.5$) for shrinking surface. It is found that for non-Newtonian case fluid adjacent to the surface and rotate due to shrinking surface. However, for Newtonian case rotating flow behavior is appear far from the shrinking surface. In Fig. 17, results are plotted for non-Newtonian case when velocity ratio parameter is $\varepsilon = -0.5$ and $\varepsilon = -1.0$. Flow distribution for $\varepsilon = -1.0$ is very high as compare to the $\varepsilon = -0.5$ case. All these results are just describing the flow distributions effects in the whole domain of the boundary layer.

Conclusion

The two-dimensional stagnation-point flow of nanofluid towards horizontal linearly stretching sheet under the effects of velocity slip and thermal radiation was studied in this paper. Numerical solution of governing differential equations is obtained using finite difference method. The flow and heat transfer characteristics were analyzed in details. The study concludes that velocity slip reduces the fluid velocity and wall skin friction. Moreover, due to increase in velocity slip the Nusselt number decreased whereas Sherwood number increased. Thermal radiation also had considerable impact on the heat transfer characteristics. Nusselt number increased and Sherwood number increased due to increase in thermal radiation.

Acknowledgments

Second author, Rizwan Ul Haq would like to acknowledge and express his gratitude to the Higher Education Commission, Pakistan for startup research grant (SRGP#1351).

Professor Qasem M. Al-Mdallal would like to acknowledge and express their gratitude to the United Arab Emirates University, Al Ain, UAE for providing the financial support with Grant No. 31S240-UPAR (2) 2016.

References

[1] BC Sakiadis, Boundary-layer behavior on continuous solid surfaces: I. Boundary layer equations for two-dimensional and axisymmetric flow.
[2] BC Sakiadis, Boundary-layer behavior on continuous solid surfaces: II. Boundary-layer on a continuous falt surface.
[3] BC Sakiadis, Boundary-layer behavior on continuous solid surfaces: III. The boundary-layer on a continuous cylindrical surface.
[4] Lawrence J. Crane, Flow Past a Stretching Plate. J Appl Math Phys 1970;21:645.
[5] Chiam T. Stagnation-point flow towards a stretching plate. J Phys Soc Japan 1994;63:2443–4.
[6] Mahapatra T, Gupta A. Heat transfer in stagnation-point flow towards a stretching sheet. Heat Mass Transfer 2002;38:517–21.
[7] Shen Ming, Wang Fei, Chen Hui. MHD mixed convection slip flow near a stagnation-point on a nonlinearly vertical stretching sheet. Boundary Value Problems 2015;2015:78.
[8] Soid Siti Khuzaimah, Merkin John, Ishak Anuar, Pop Ioan. Axisymmetric stagnation-point flow and heat transfer due to a stretching/shrinking vertical plate with surface second-order velocity slip. Meccanica 2017;52:139–51.
[9] Animasaun IL, Prakash J, Vijayaragavan R, Sandeep N. Stagnation flow of nanofluid embedded with dust particles over an inclined stretching sheet with induced magnetic field and suction. J Nanofluids 2017;6:1–10.
[10] Naveed M, Abbas Z, Sajid M. MHD flow of micropolar fluid due to a curved stretching sheet with thermal radiation. J Appl Fluid Mech 2016;9(1):131–8.
[11] Stephen US Choi, JA Eastman, Enhancing thermal conductivity of fluids with nanoparticles, ASME International Mechanical Engineering Congress and Exposition, November 1995, San Francisco, CA.
[12] Kwak Kiyuel, Kim Chongyoup. Viscosity and thermal conductivity of copper oxide nanofluid dispersed in ethylene glycol. Korea-Aust Rheol J 2005;17(2):35–40.
[13] Wong Kuafui V, De Leon Omar. Applications of nanofluids: current and future. Adv Mech Eng 2010;519659.
[14] Khan WA, Pop I. Boundary-layer flow of a nanofluid past a stretching sheet. Int J Heat Mass Transfer 2010;53:2477–83.
[15] Haq Riwan Ul, Nadeem Sohail, Khan Zafar Hayat, Akbar Noreen Sher. Thermal radiation and slip effects on MHD stagnation-point flow of nanofluid over a stretching sheet. Phys E 2015;65:17–23.
[16] Rashid Irfan, Haq Rizwan Ul, Al-Mdallal Qasem M. Aligned magnetic field effects on water based metallic nanoparticles over a stretching sheet with PST and thermal radiation effects. Phys E 2017;89:33–42.
[17] Haq Rizwan Ul, Rajotia D, Noor NFM. Thermo physical effects of water driven copper nanoparticles on MHD axisymmetric permeable shrinking sheet: Dual-nature study. Eur Phys J E 2016;39.
[18] Haq Rizwan Ul, Khan ZH, Khan WA, Shah Inayat Ali. Viscous dissipation effects in water driven carbon nanotubes along a stream wise and cross flow direction. Int J Chem Reactor Eng 2016.
[19] Fukui S, Kaneko R. A database for interpolation of poiseuille flow rates for high knudsen number lubrication problems. J Tribol 1990;112:78–83.
[20] Mitsuya Y. Modified reynolds equation for ultra-thin film gas lubrication using 1.5-order slip-flow model and considering surface accommodation coefficient. J Tribol 1993;115:289–94.
[21] Maxwell JC. On stresses in rarified gases arising from inequalities of temperature. Philos Trans R Soc 1879;170:231–56.
[22] Lin Wu. A slip model for rarefied gas flows at arbitrary Knudsen number. Appl Phys Lett 2008;93:253103.
[23] Lin Wu. A slip model for rarefied gas flows above a moving surface with mass transfer. J Appl Phys 2014;116:054503.
[24] Hayat T, Shafiq A, Asaedi A, Shahzad SA. Unsteady MHD flow over exponentially stretching sheet with slip conditions. Appl Math Mech 2016;37(2):193–208.

[25] Abdul Hakeem AK, Renuka P, Vishnu Ganesh N, Kalaivanan R, Ganga B. Influence of inclined Lorentz forces on boundary layer flow of Casson fluid over an impermeable stretching sheet with heat transfer. J Magnet Magnet Mater 2016;401:354–61.
[26] Prasannakumara BC, Gireesha BJ, Rama, Gorla SR, Krishnamurthy MR. Effects of chemical reaction and nonlinear thermal radiation on Williamson nanofluid slip flow over a stretching sheet embedded in a porous medium. J Aerospace Eng 2016;29(5):04016019.
[27] Dogonchi Abdul Sattar, Ganji Davood Domiri. Thermal radiation effect on the nanofluid buoyancy flow and heat transfer over a stretching sheet considering Brownian motion. J Mol Liq 2016;223:521–7.
[28] Chen Hui, Liang Hongxing, Wang Fei, Shen Ming. Unsteady MHD stagnation-point flow towards a shrinking sheet with thermal radiation and slip effects. Heat Transfer-Asian Res 2016;48(8):730–45.
[29] Ullah Imran, Khan Ilyas, Shafie Sharidan. MHD natural convection flow of Casson nanofluid over nonlinearly stretching sheet through porous medium with chemical reaction and thermal radiation. Nanoscale Res Lett 2016;11:527.
[30] Abdel-wahed Mohamed S. Nonlinear Rosseland thermal radiation and magnetic field effects on flow and heat transfer over a moving surface with variable thickness in a nanofluid. Can J Phys 2016;95:267–73.
[31] Rana S, Mehmood R, Narayana PVS, Akbar NS. Free convective nonaligned non-Newtonian flow with nonlinear thermal radiation. Commun Theor Phys 2016;66:687–93.
[32] Rosseland S. Astrophysik and Atom-Theorestischegrundlagen. Berlin: Springer; 1931.
[33] Makinde OD, Aziz A. Boundary layer flow of a nanofluid past a stretching sheet with a convective boundary condition. Int J Thermal Sci 2011;50:1326–32.